

Short Communication

Investigation of HRB335 steel Corrosion in Concrete in Chloride-Containing Sulfate Solution Using Electrochemical Method

Jianrong Pang, Guosong Shi*, Gang Li, Yanmeng Qi

College of Civil Engineering, Cangzhou Jiaotong College, Hebei Cangzhou 061199, China

*E-mail: shi_teacher00@126.com

Received: 2 September 2021 / *Accepted:* 14 October 2021 / *Published:* 10 November 2021

High mechanical strength, long durability, and other outstanding characteristics make concretes widely used in the construction of bridges, buildings, sewage pipeline, and many more infrastructure items. However, in the long run, micro-cracking and chloride ion diffusion caused by the corrosion of steel reinforcement exert a hazardous effect on the properties of concretes, which has aroused special attention of the scholars. In this work, the failure mechanism of concrete induced by chlorine-containing sulfate corrosion is studied via array electrode technology, electrochemical experiments, and corrosion morphology analysis. The results show that the failure caused by the corrosive medium diffusion in the cracks inside the concrete can be divided into two stages. First, the corrosive medium reaches the concrete - reinforcement surface and forms a corrosion galvanic cell with a large cathode and a small anode, which promotes the corrosion product accumulation. Second, the Cl⁻ ions destroy the corrosion product layer and make the rust spread to the inside of concrete, while leading to severe pitting corrosion of the metal matrix.

Keywords: Concrete; Cl⁻-containing sulfate; Array electrode; Electrochemical method

1. INTRODUCTION

Concrete occurred more than 150 years ago, becoming the most widely used artificial material due to its excellent performance in construction [1,2]. However, there are still a lot of problems associated with the durability of concrete, which lead to the destruction of the whole structure of the item, causing huge economic losses [3].

The research on concrete durability mainly consists in monitoring salt corrosion, freeze-thaw damage, carbonization, alkali aggregate reactions, etc. Salt corrosion is mainly induced by the sulfate chlorides and takes place in predominately hydraulic structures, coastal buildings and underground

structures. This type of corrosion in concretes is a relatively complex process, leading to physical and chemical damage of their structure. Sulfate corrosion mainly causes expansion and cracking of concrete [4]. When concrete cracks, its permeability increases and the corrosion medium easier infiltrates into the interior. This, in turn, speeds up the structural deterioration and leads to the loss of cohesion between cement hydration products. Under this circumstance, the concrete is manifested by gradually decreasing strength and mass loss [5].

The research on concrete in sulfate environment aims to mainly gain insight into the mechanism of sulfate corrosion. Sulfate corrosion in concretes is a complex process that includes both physical corrosion and chemical corrosion. Tennich et al. [6] carried out the dry-wet cycle experiment of the concrete mixed with breeze in 5 wt % Na_2SO_4 solution to study their dynamic modulus of elasticity, compressive strength, amplitude of variation characteristics. According to the results, the dynamic elastic modulus first declined and then rose to a stable value, finally dropping to the failure level. The amplitude remained unchanged in the first 100 dry-wet cycles, after which it continued to go down until the specimen failed [7]; in turn, the compressive strength decreased by 28%-62%. Gao et al. [8] studied the effect of fly ash addition on the sulfate corrosion in concrete, observing the reduction of the corrosive components along with the formation of ettringite and gypsum [9] and, consequently, the improvement in the corrosion resistance of the material. Cefis et al. [10] performed the accelerated corrosion test of high-strength concrete in sodium sulfate solution. After corrosion by sodium sulfate, the strength of the concrete first increased and then decreased, while the quality exhibited an opposite trend.

Concrete is a complex composite material with a multi-scale sub-continuous structure. The microstructure of concrete includes voids, reinforcing agents, mortar, and the interfaces between them. The microstructure plays a key role in the behavior of concrete at the macroscopic level. In the past few decades, numerous efforts have been made to improve the corrosion resistance of concretes. In particular, many mesoscopic models have been proposed and developed to understand and quantify the effects of microstructure and local failure mechanisms on the long-term response of concretes [11]. In the context of the meso-structural model, the shape and size of mortar exert influence on the stress distribution, crack initiation and damage accumulation in the concrete until the macroscopic failure. Furthermore, various scholars have reported the numerical models to analyze the deterioration process of concretes from different perspectives; but few of them monitored the failure process based on the corrosion behavior of reinforcing agents in concrete [12]. Therefore, in present work, wire electrode technology, electrochemical testing and corrosion image analysis were used to study the reinforcement corrosion and failure degradation caused by the internal diffusion in concrete. The findings of this research enabled one to reveal the failure degradation mechanism of concrete and improve its durability.

2. EXPERIMENT SETTINGS

(1) Experimental materials. The information about the main components and HRB335 steel as the reinforcing agent applied in this study is available in Table 1.

Table 1. Main components of HRB335 steel (wt.%)

Element	C	Si	Mn	P	S	Fe
Content	0.25	0.80	1.60	0.045	0.045	0.52

(2) Preparation of array electrodes. Using a transparent plexiglass panel, 10×10 array round holes were obtained by a fine engraving machine with the aperture of 2 mm; the spacing between the holes was 0.5 mm. After that, polished HRB335 metal wires with 2-mm diameters were inserted into the holes to make sure the electrodes were parallel to the plexiglass plate. The array electrodes were encapsulated with epoxy resin to achieve complete insulation between the wires. After curing at room temperature for 72 h, the array electrodes were polished to make the HRB335 metal matrix completely out. Then, the electrodes were polished with a metallographic sandpaper to reduce the experimental error caused by different surface roughness. Finally, the treated array electrodes were put into a vacuum drying oven for later use. A schematic of such an array electrode is shown in Fig. 1.

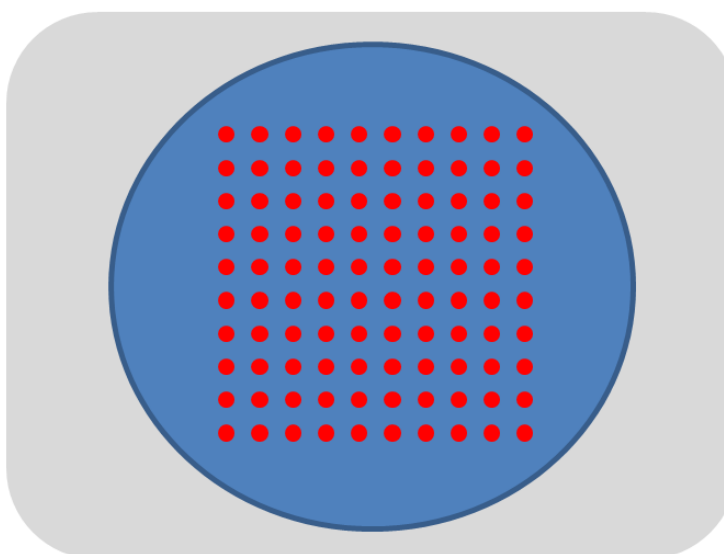


Figure 1. Section diagram of array electrode

(3) Preparation of concrete layer. Portland cement (P.O42.5), sand with a mud content of less than 3%, and gravel with a particle size of 5-20 mm were used as raw materials [13] to make concrete with respect to the formula in Table 2. A plastic cylinder with a diameter of 5 cm was incorporated into the outer part of the filament electrode to completely cover it. Finally, concrete was added to the cylinder and solidified at room temperature for 7 days.

Table 2. Experimental concrete formulation

Water cement ratio	Sand ratio	Cement (kg·m ³)	Sand (kg·m ³)	Stone (kg·m ³)
0.76	0.498	319	915	922

(4) Experimental conditions. The experimental solution was prepared with analytically pure NaCl, Na₂SO₄ and deionized water with a mass fraction of 3.5%, so that NaCl and Na₂SO₄ contents were 0.5% and 3%, respectively. The experimental temperature was 25°C, and the whole experimental device was placed in a box with constant temperature and humidity to reduce the influence of environmental factors on the experimental results.

(5) Data collection. A Pt electrode served as the auxiliary electrode, whereas a saturated calomel electrode (SCE) was used as the reference electrode. LabView software was applied to realize the automatic collection of array electrode potential and current density values under different experimental time conditions through a data acquisition card. The experimental period was 72 h.

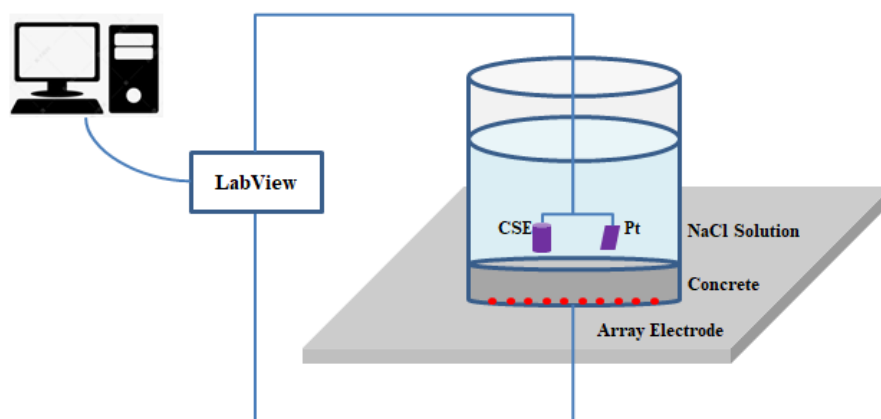


Figure 2. Experimental device for surface potential and current density acquisition

(6) Immersion experiment. Based on Fig. 2, a HRB335 sample with dimensions of 10×10×2 mm³ was used to replace the wire electrode system to carry out the immersion experiments. The microstructure of concrete undergoing failure was analyzed according to the test results of array electrodes. The corrosion morphology of the HRB335 sample was observed by Zeiss microscope after removing the surface concrete and corrosion products.

(7) EIS testing. The EIS testing was performed on the above HRB335 sample. A PARSTAT 2273 electrochemical workstation was employed instead of LabView one. The trials were carried out in a frequency range of 10⁵-10⁻² Hz and the disturbance voltage of ±10 mV. Data were processed using ZSimpWin software.

3. RESULTS AND DISCUSSION

3.1 Surface electrochemical parameter analysis

Fig. 3 displays the surface potential and current density distribution of steel in concrete as functions of time. In turn, Fig. 4 depicts the potential distribution on the surface of the steel in concrete

after immersing 3 h, whereas Fig.5 shows the anode-cathode potential difference and the average current density of steel in concrete varying with time.

The diffusion of a corrosive medium in concrete depends on the two aspects. First, due to the structure of concrete itself, there is a large number of cracks. At the initial stage of the immersion experiment, the corrosive medium gradually reaches the concrete-steel surface through the cracks, which corresponds to a failure site. Second, when the experiment is completed, the corrosive medium continuously destroys the concrete in the diffusion process, weakening the compactness of the material and resulting in the direct exposure of the array electrode to the corrosive environment. Therefore, the diffusion of the corrosive medium in concrete will inevitably lead to the existence of failure sites, that is, the corrosive medium first arrives at the concrete-steel surface [14-16]. According to the plots in Fig. 4, the maximum positive potential after 3 h emerged at the position (2,8), corresponding to a value of -0.691 V, while the most negative positions appeared at the points (9,4) (9,5) and (9,9), being attributed to -0.708 V. This means that the corrosive medium at the (2,8) coordinate point could have reached the array-electrode surface first, while three positions with the most negative potentials could have indicated intact protective characteristics of concrete [17]. The steel in concrete with a corrosion potential of -0.708 V at the position of other array electrode relative to the initial moment had different degrees of positive deviation, indicating that the diffusion process of the corrosive medium in concrete had started, and the greater the positive deviation degree, the higher the diffusion degree [18].

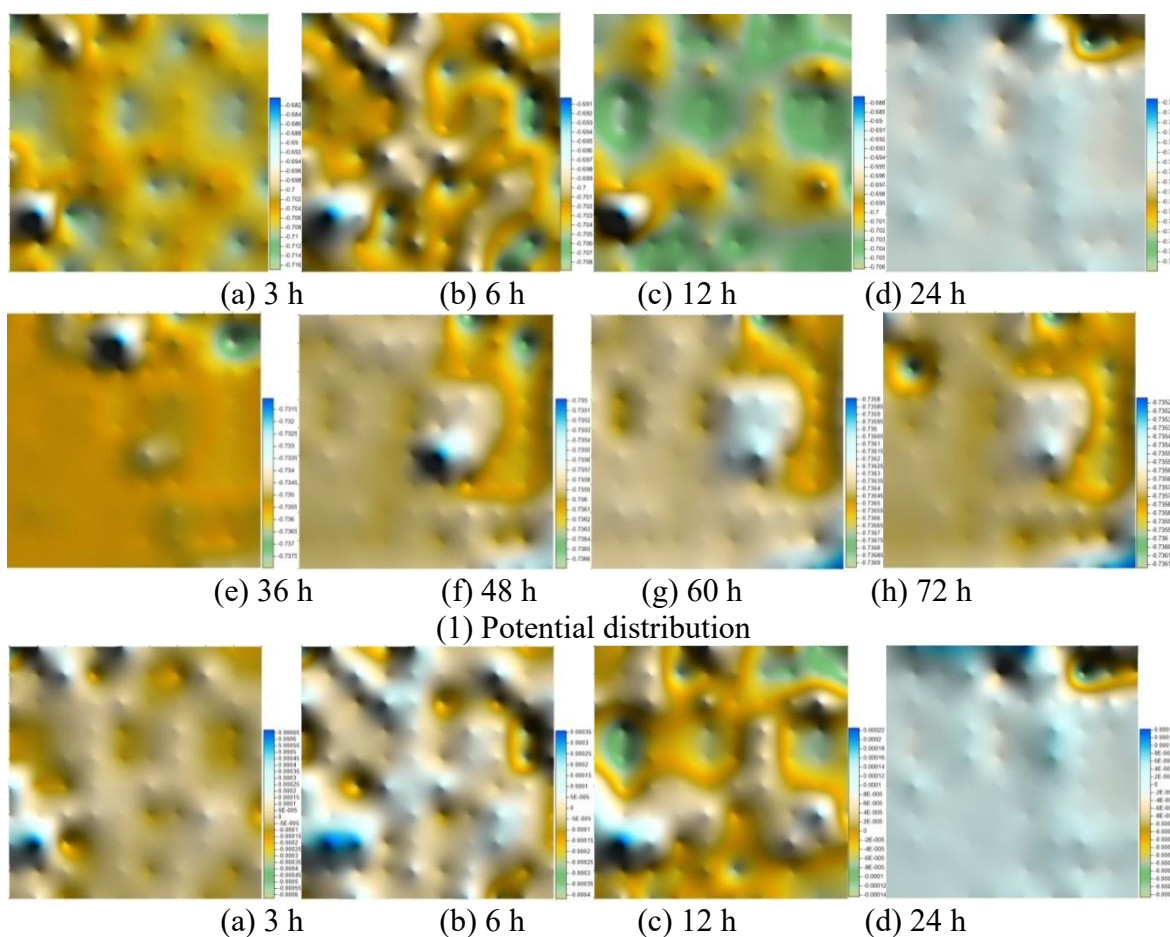
In the course of the experiment, the potential distribution of the steel in concrete at the time period of 6 h became more uneven, and the maximum potential difference was as high as 34 mV. Compared with the potential distribution image after 3 h, the anode area remained basically unchanged, while the potential in the cathode area exhibited the mostly positive deviation, except for some local sites. This means that the potential distribution within the large cathode and small anode areas tended to be balanced gradually. At the experiment time of 12 h, the corrosive medium had comprehensively reached the interface of the array electrode, and the potential of the cathode area experienced a pronounced positive deviation.

When the corrosive medium achieves the surface of the local electrode, under this condition, activation corrosion occurs first. However, if the oxygen on the concrete-steel interface was exhausted, the oxygen concentration cell was formed to continue to promote a continuous local pitting process due to the block of the concrete-steel interface [19-22]. Therefore, when the experimental time increases from 3 to 6 h, the potential at the point (2,8) continued to shift positively, and the potential difference between the cathode and the anode enriched its maximum. After 24 h of the experiment, the potential of the whole steel in concrete had a significant negative shift, and the surface potential distribution ranged from -0.722 V to -0.738 V. Meanwhile, in the following 48 h, the surface potential of the steel in concrete basically remained unchanged.

Exposing the material to 12 h of the experiment resulted in a high content of corrosive media on the surface of the array electrodes and the electrochemical corrosion of the interface. At this time, most of corrosion products at the interface diffused into the interior of the concrete, aggravating the deterioration of the latter [23]. Therefore, the whole steel in concrete underwent a noticeable negative potential deviation at a later moment and then remained unchanged for a long period of time.

The current density distribution of the array electrodes showed the same trend. As the experiment progressed, well-pronounced cathodes and anodes appeared in the array electrode, where the regions with the corrosive medium were referred to as anodes. An increase in time from 3 to 6 h led to a drastic increase in the maximum cathode/anode potential difference as well as in the current density of the anode and cathode, which was caused by their general equilibrium. After 24 h of the experiment, the current density distribution on the surface became more uniform and remained basically unchanged in the following 48 h, which was owing to the corrosion products blocking the diffusion channel at the interface and thus promoting the deterioration of concrete [24].

Analyzing the changes in surface potential and current density distribution with time, it can be seen that the failure of concrete can be divided into two stages. First, the corrosive medium reaches the surface of the array electrodes and forms a corrosion galvanic cell with a large cathode and a small anode, which promotes the corrosion on the concrete-steel surface [25]. Second, corrosion products diffuse into the interior of the concrete, accelerating the deterioration of the latter. Therefore, the cathode-anode potential difference and the average current density both decreased with the experiment time (Fig. 5).



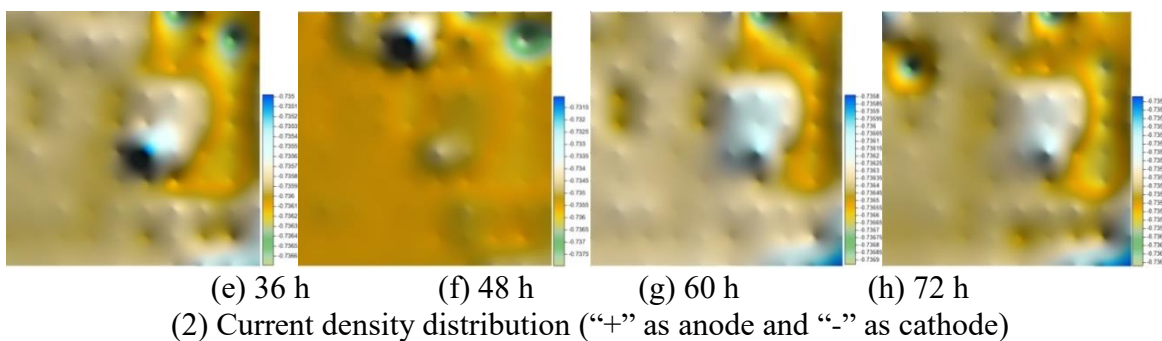


Figure 3. The variation of surface potential and current density distribution of HRB335 steel in concrete with time

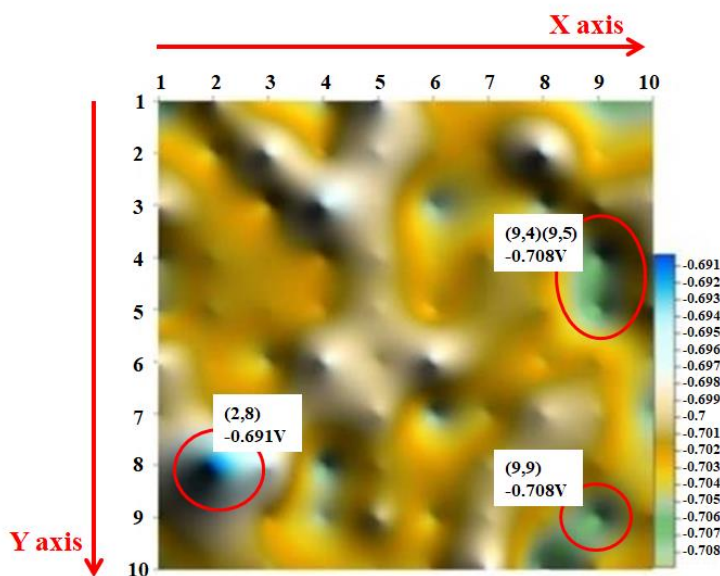


Figure 4. The potential distribution on the surface of the HRB335 steel in concrete at 3 h

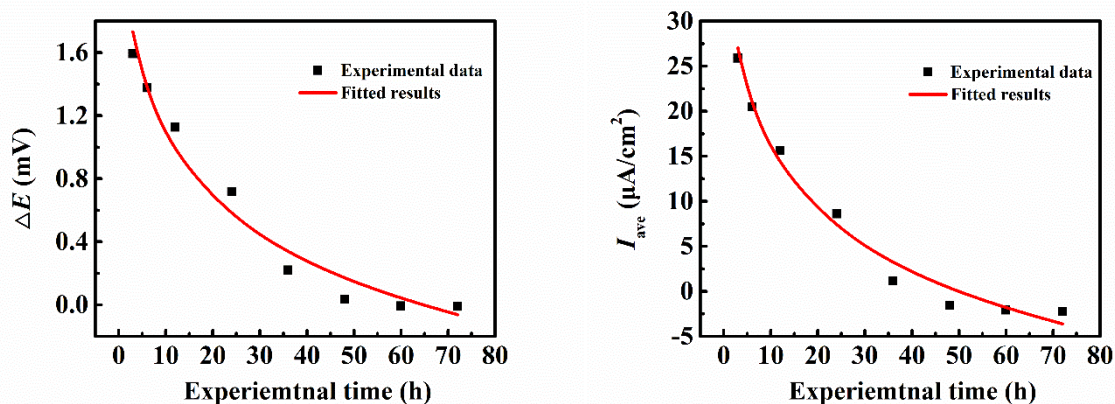


Figure 5. The variation of the potential difference of anode - cathode and the average current density of HRB335 steel in concrete with time

3.2 Corrosion morphology analysis

The immersion experiment was carried out to analyze the surface morphology of the steel in concrete. Fig. 6 displays the microscopic morphology of the failure site after 3 h of immersion. In turn, Fig. 7 depicts the corrosion morphology of the metal surface after immersion for 72 h and after removing the anticorrosive layer.

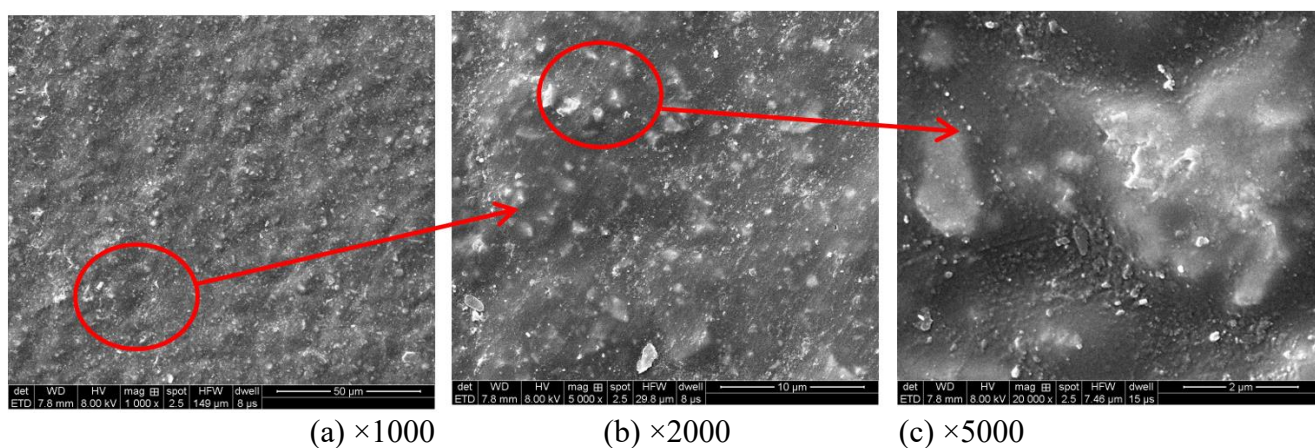


Figure 6. Surface morphology of the steel in concrete when immersion for 3 h

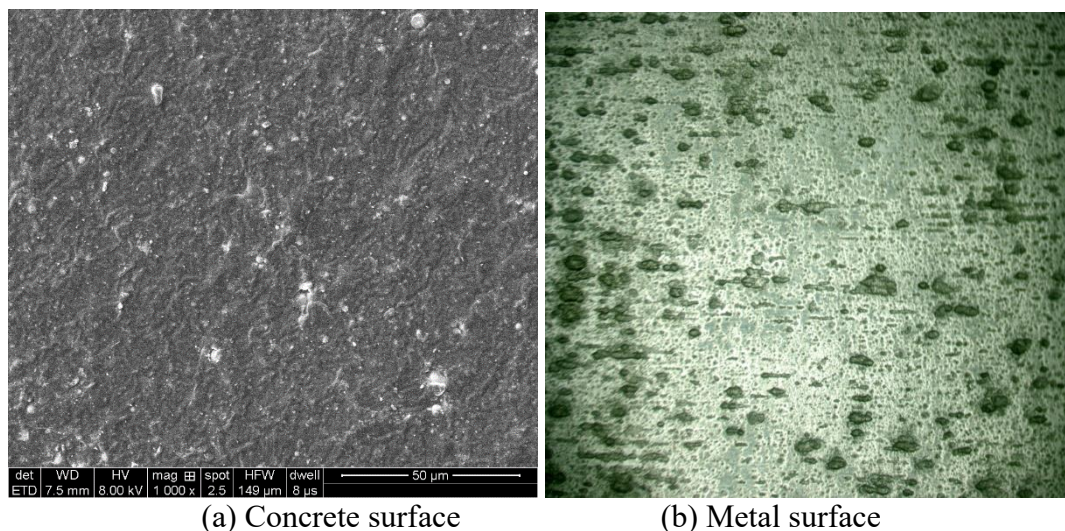


Figure 7. Morphology of steel in concrete and metal surface for 72 h

According to Fig. 6, the surface morphology of the steel in concrete was relatively smooth and uniform, without remarkable changes at the local level ($\times 1000$). From the local magnification of the surface topography ($\times 2000$), it can be seen that the color of some positions changed from black to white. Furthermore, the $\times 5000$ magnification revealed dramatic differences in the positions from the surrounding sites. In particular, the local thickness increased, resulting in the bright white color of the corresponding areas, which was attributed to the diffusion of the corrosive medium toward the

concrete-reinforcement interface. In turn, the occurrence of the electrochemical reaction led to the change of the concrete thickness [26,27].

With the increase of immersion time to 72 h (Fig. 7), the concrete surface had no obvious change compared with that after 3 h. From the above analysis, when the immersion time was increased to 72 h, a large amount of the corrosive medium had reached the concrete-reinforcement interface, and the electrochemical corrosion process of the interface was fully developed. After removing the surface concrete and corrosion products, the metal surface exhibited the signs of severe pitting corrosion.

3.3 EIS analysis

Fig. 8 depicts the EIS characteristics of the steel in concrete, varying with time. In turn, Table 3 shows the equivalent circuit fitting parameters at different immersion times.

Once the corrosive medium arrived at the surface of HRB335 steel, activation corrosion became the main electrochemical reaction, leading to the accumulation of the corrosion products on the metal surface [28]. As a result, a complete capacitive arc in the Nyquist diagram could be observed. When the immersion time was prolonged, the Cl^- ions penetrated the corrosion product film, yielding a dramatic decrease in the radius of the Nyquist plot at 6 and 12 h. No other reactions, however, occurred on the metal surface. Therefore, the equivalent circuit $R_s(QR_p)$ was selected within a range of 0-12 h, in which R_s is the solution resistance, Q is the system capacitance, and R_p is the polarization resistance. At this stage, according to Table 3, the polarization resistance (R_p) of the steel in concrete was $3.435 \times 10^4 \Omega \cdot \text{cm}^2$, gradually decreasing to $1.161 \times 10^4 \Omega \cdot \text{cm}^2$ as the diffusion progressed. At the same time, the system capacitance increased from 1.399×10^{-5} to $4.256 \times 10^{-5} \text{ F/cm}^2$. As mentioned above, this was because the complete corrosion product film on the metal surface was destroyed by the Cl^- induced corrosion. Moreover, there were multiple local resistors on the metal surface, connected in parallel, resulting in a decrease in the total polarization resistance of the whole surface. However, a series of local capacitors increased the capacitance of the entire system, and the dispersion index ($n = 0.51-0.59$) remained basically unchanged. This indicates that the roughness of the concrete surface was equal to degree of uniformity of the corrosion current density at different test times, which had no influence on the test results [29,30].

When the experiment was carried out for 18 h, the Nyquist diagram of the steel in concrete exhibited obvious double capacitance resistance characteristics, meaning that there were simultaneously two time constants [31]. The first constant represented the corrosion process associated with Cl^- ions on the metal surface, whereas the second one was attributed to the damage of Cl^- ions on the corrosion product film and the diffusion of the corrosion products toward the interior of the concrete. However, due to the limitation of the internal structure of concrete, the diffusion of corrosion products had a certain blocking effect owing to a finite layer diffusion process. Therefore, $R_s(Q(R_pO(C_{dl}R_{ct}))$ was selected as the equivalent circuit, in which R_s is the solution resistance, Q is the system capacitance, R_p is the polarization resistance, O is the effective layer capacitance, C_{dl} is the double layer capacitance, and R_{ct} is the charge transfer resistance.

As can be seen from the Nyquist diagram, the impedance radius of the real part of the material diffusion after 18 h of immersion decreased greatly under the double capacitive reactance characteristics [32]. This was because the Cl⁻ ions damaged the corrosion film layer, increasing the concentration of loose corrosion products on the metal surface, which reduced the diffusion resistance of the concrete. With a further increase in the immersion time to 24 h, the diffusion characteristic of the finite layer completely disappeared, being replaced by Weber diffusion impedance. At the same time, the shape of the Nyquist plot did not change in the following 12 h, and the whole reaction process was mainly characterized by the activation corrosion of metal. Therefore, the equivalent circuit was $R_s(Q(R_p W(C_{dl} R_{ct})))$, where R_s is the solution resistance, Q is the system capacitance, R_p is the polarization resistance, W is the Weber diffusion resistance, C_{dl} is the double layer capacitance, and R_{ct} is the charge transfer resistance.

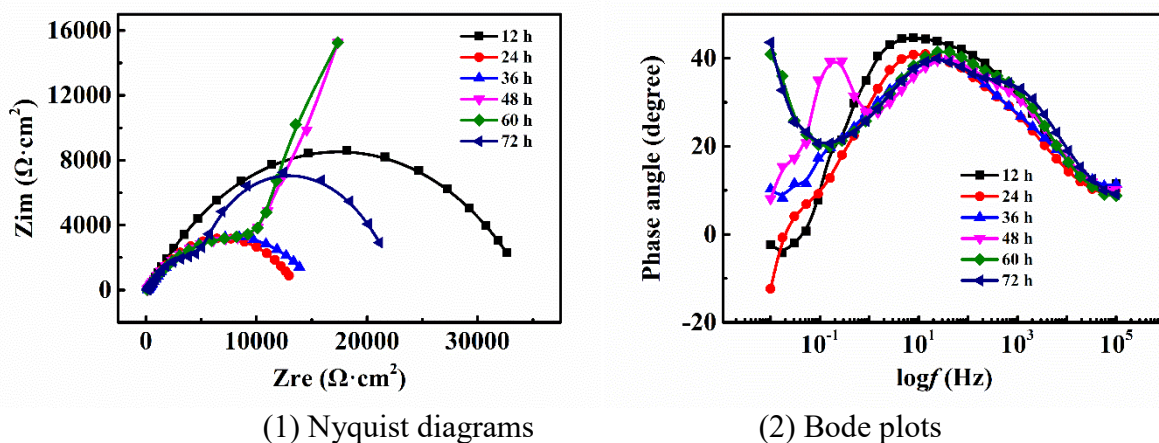


Figure 8. The change curves of EIS characteristics of steel in concrete with time

Table 3. Fitted results of equivalent electric circuits

Time Parameter	12 h	24 h	36 h	48 h	60 h	72 h
R_s ($\Omega \cdot \text{cm}^2$)	269.9	184.7	157.5	141	129.5	117.7
Q (F/cm^2)	1.399	3.303	4.256	2.48	3.443	3.966
n	0.59	0.56	0.51	0.56	0.55	0.51
R_p ($\Omega \cdot \text{cm}^2$)	3.435	1.54	1.161	0.2035	1.273	1.413
O (F/cm^2)	-	-	-	2.588	-	-
B	-	-	-	0.142	-	-
W ($\Omega \cdot \text{cm}^2$)	-	-	-	-	1.162	2.98
C_{dl} (F/cm^2)	-	-	-	8.601	87.48	75.28
R_{ct} ($\Omega \cdot \text{cm}^2$)	-	-	-	1.554	2.714	5.115

In the Bode plots, the phase angle was divided into the three distinct stages. In the first stage (0-12 h), the curve contained a single peak, indicating that there was only one time constant associated with the metal activation corrosion. During the experiment, the maximum phase angle slightly

decreased ($44.7^\circ \rightarrow 41^\circ \rightarrow 39.9^\circ$), whereas the corresponding maximum frequency gently increased ($7.9 \rightarrow 13.7 \rightarrow 24$ Hz) [33,34]. The results revealed that the corrosion effect of Cl^- on the dense corrosion product film became stronger. Furthermore, two obvious time constants appeared at 18 h, indicating that the corrosion products diffused from the surface of HRB335 steel to the inside of concrete, accelerating the failure of the latter. However, in the final stage (24-36 h), the "peak" of the double layer dramatically shifted to the low frequency range, while the maximum phase angle and frequency remained unchanged by analogy with their behavior at the second stage. These findings agreed with the Nyquist diagram.

4. CONCLUSION

In this work, the combination of array electrode technology and electrochemical impedance spectroscopy enabled one to monitor the failure process caused by the diffusion of the corrosive medium in concrete. Based on the results, the main conclusions can be drawn as follows.

(1) The failure caused by the corrosive medium diffusion in the cracks inside the concrete could be divided into two stages. First, the corrosive medium reached the surface of the wire electrode and formed a corrosion galvanic cell with a large cathode and a small anode, which promoted the reaction process on the concrete-reinforcement surface. Second, corrosion products were spreading inside the concrete structure, accelerating its deterioration. Therefore, the cathode-anode potential difference and average current density decreased in the course of the experiment.

(2) The EIS testing revealed that the damage of concrete, induced by chlorinated sulfate, could be described by the two-stage process. As soon as the corrosive medium achieved the metal surface, the corrosion process occurred, yielding the corrosion products accumulation and the formation of the corrosion layer on the concrete-reinforcement surface. Moreover, the small radii of Cl^- ions allowed them to penetrate the corrosion product film and enrich the surface of the metal matrix. On the one hand, the corrosion layer was destroyed and the corrosion products were spreading in the inside of concrete, resulting in the expansion and rupture of the material. On the other hand, Cl^- ions caused severe pitting of the metal matrix.

ACKNOWLEDGEMENTS

This study is supported by the the Key Research and Development Project of Cangzhou Municipal Science and Technology Bureau, China (Grant No.192107005) and Teaching Research Project of Beijing Jiaotong University Haibin College, China (Grant No. HBJY19021).

Reference

1. E.F. Irassar, A. Di, Maio and O.R. Batic, *Cement Concrete Res.*, 26 (1996) 113.
2. S. Lorente, M.P. Yssorche-Cubaynes and J. Auger, *Cement & Concrete Comp.*, 33 (2011) 735.
3. C. Yang, Q. Han, A.Q. Wang, Y. Yang and X.Y. Li, *AIP Adv.*, 11 (2021) 035217.
4. T. Liu, D. Zou, J. Teng and G. Yan, *Constr. Build. Mater.*, 28 (2012) 201.
5. F. Varela, M.Y.J. Tan and M. Forsyth, *Electrochim. Acta*, 186 (2015) 377.

6. M. Tennich, M.B. Ouezdou and A. Kallel, *Constr. Build. Mater.*, 135 (2017) 335.
7. W. Vélez, F. Matta, P. Ziehl, *Mater. Struct.*, 49 (2016) 507.
8. F.F. Gao, W. Tian, Y. Wang and F. Wang, *Struct. Concrete*, 22 (2020) 955.
9. B. Elsener, D. Addari, S. Coray and A. Rossi, *Mater. Corros.*, 62 (2011) 111.
10. N. Cefis and C. Comi, *Cement Concrete Res.*, 93 (2017) 57.
11. I. Gurrappa, I.V.S. Yashwanth and I. Mounika, *P. Natl. A. Sci. India A.*, 85 (2015) 1.
12. A. Thybo, A. Michel and H. Stang, *Mater. Struct.*, 50 (2018) 146.
13. C. Xu, F. Gao, Y. Wang and C. He, *Mater. Design*, 89 (2016) 196.
14. P.J. Tumidajski, G.W. Chan and K.E. Philipose. *Cement Concrete Res.*, 25 (1995) 1159.
15. M. Oleiwi, W. Yu, M. Curioni, X. Chen and I.L. Shabalina, *Mater. Struct.*, 51 (2018) 148.
16. M. Zhang, J. Chen, Y. Lv, D. Wang and Y. Jian, *Constr. Build. Mater.*, 39 (2013) 26.
17. A. Goyal, H.S. Pouya, E. Ganjian, A.O. Olubanwo and M. Khorami, *Constr. Build. Mater.*, 194 (2019) 344.
18. M.J. Shannag and H.A. Shaia, *Cement & Concrete Comp.*, 25 (2003) 363.
19. J. Shen, G.L. Song, D.J. Zheng and Z.M. Wang, *Mater. Corros.*, 70 (2019) 2228.
20. C. Sun, J.K. Chen, J. Zhu, M.H. Zhang and J. Ye, *Constr. Build. Mater.*, 39 (2013) 39.
21. P.J. Tumidajski and I. Turc, *Cement Concrete Res.*, 25 (1995) 924.
22. G.S. Steeb and R. Tank, *Mater. Corros.*, 60 (2015) 344.
23. Z.Liu, D. Deng and G.D. Schutter, *Constr. Build. Mater.*, 66 (2014) 692.
24. F.M. Song, *Corros. Sci.*, 55 (2012) 107.
25. B.S. Mindess, *Cement Concrete Res.*, 34 (2004) 373.
26. C. Jiang, Y.F. Wu and M.J. Dai, *Constr. Build Mater.*, 158 (2018) 1073.
27. S. Kumar and C. Rao, *Cement Concrete Res.*, 25 (1995) 57.
28. A. Husain, J. Chakkamalayath and S. Al-Baha, *Eng. Fail. Anal.*, 82(2017)765.
29. J.W. Oldfield and W.H. Sutton, *Br. Corros. J.*, 13(1989)104.
30. C.G. Oliveira and M.G.S. Ferreira, *Corros. Sci.*, 123(2003)45.
31. L. Caceres, T. Vargas and M. Parra, *Electrochim. Acta*, 7435(2009)54.
32. H. Tanaka, R. Mishima, N. Hatanaka, T. Ishikawa and T. Nakayama, *Corros. Sci.*, 78(2014)384.
33. P. Dillmann, R. Balasubramaniam and G. Beranger, *Corros. Sci.*, 44(2002)2231.
34. F.F. Eliyan, E.S. Mahdi and A. Alfantazi, *Corros. Sci.*, 58(2012)181.

© 2021 The Authors. Published by ESG (www.electrochemsci.org). This article is an open access article distributed under the terms and conditions of the Creative Commons Attribution license (<http://creativecommons.org/licenses/by/4.0/>).